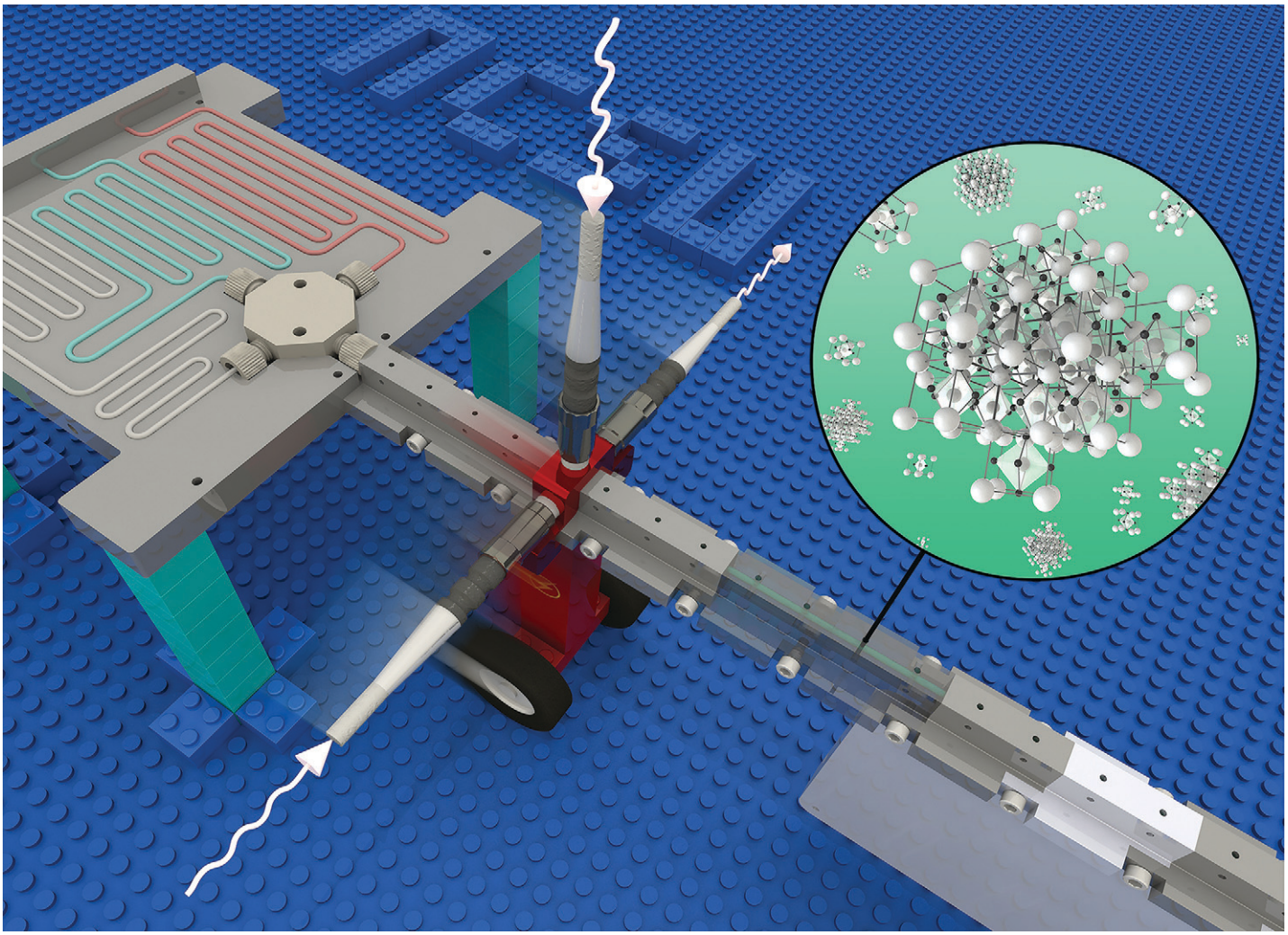

Featuring work from the Abolhasani Lab of the Department of Chemical and Biomolecular Engineering at North Carolina State University, which focuses on developing flow chemistry strategies towards addressing the environmental challenges of the growing global energy demand.

Automated microfluidic platform for systematic studies of colloidal perovskite nanocrystals: towards continuous nano-manufacturing

A modular microfluidic technology for systematic studies of colloidal nanocrystals is developed and applied towards high-throughput screening of perovskite quantum dots. The developed translational flow cell module allows in-line spectral monitoring of the colloidal nanocrystals along the reactor without affecting the early stage mixing time of precursors.

As featured in:

See Milad Abolhasani *et al.*, *Lab Chip*, 2017, **17**, 4040.

ROYAL SOCIETY OF CHEMISTRY

rsc.li/loc

Registered charity number: 207890

Lab on a Chip

PAPER

View Article Online
View Journal | View Issue

Cite this: *Lab Chip*, 2017, **17**, 4040

Automated microfluidic platform for systematic studies of colloidal perovskite nanocrystals: towards continuous nano-manufacturing†

Robert W. Epps, [a] Kobi C. Felton, [a] Connor W. Coley [b] and Milad Abolhasani *[a]

Colloidal organic/inorganic metal-halide perovskite nanocrystals have recently emerged as a potential low-cost replacement for the semiconductor materials in commercial photovoltaics and light emitting diodes. However, unlike III–V and IV–VI semiconductor nanocrystals, studies of colloidal perovskite nanocrystals have yet to develop a fundamental and comprehensive understanding of nucleation and growth kinetics. Here, we introduce a modular and automated microfluidic platform for the systematic studies of room-temperature synthesized cesium–lead halide perovskite nanocrystals. With abundant data collection across the entirety of four orders of magnitude reaction time span, we comprehensively characterize nanocrystal growth within a modular microfluidic reactor. The developed high-throughput screening platform features a custom-designed three-port flow cell with translational capability for *in situ* spectral characterization of the in-flow synthesized perovskite nanocrystals along a tubular microreactor with an adjustable length, ranging from 3 cm to 196 cm. The translational flow cell allows for sampling of twenty unique residence times at a single equilibrated flow rate. The developed technique requires an average total liquid consumption of 20 μL per spectra and as little as 2 μL at the time of sampling. It may continuously sample up to 30 000 unique spectra per day in both single and multi-phase flow formats. Using the developed plug-and-play microfluidic platform, we study the growth of cesium lead trihalide perovskite nanocrystals through *in situ* monitoring of their absorption and emission band-gaps at residence times ranging from 100 ms to 17 min. The automated microfluidic platform enables a systematic study of the effect of mixing enhancement on the quality of the synthesized nanocrystals through a direct comparison between single- and multi-phase flow systems at similar reaction time scales. The improved mixing characteristics of the multi-phase flow format results in high-quality perovskite nanocrystals with kinetically tunable emission wavelength, ranging as much as 25 nm at equivalent residence times. Further application of this unique platform would allow rapid parameter optimization in the colloidal synthesis of a wide range of nanomaterials (*e.g.*, metal or semiconductor), that is directly transferable to continuous manufacturing in a numbered-up platform with a similar characteristic length scale.

Received 15th August 2017,
Accepted 18th October 2017

DOI: 10.1039/c7lc00884h

rsc.li/loc

Introduction

Over the past two decades, colloidal semiconductor nanocrystals, known as quantum dots (QDs), (*e.g.*, CdSe, ZnS, InP, and organic/inorganic perovskite) have been extensively explored for device-level applications in solution processed photovoltaics and light emitting diodes.[1–12] While the synthesis (nucleation and growth) of II–VI and III–V QDs has been extensively characterized, a fundamental and complete understanding of the next generation of QDs – such as organic/inorganic halide perovskite QDs – has yet to be established. Comprehensive characterization of the reaction kinetics for these groups as well as continuous inline optimization to account for batch-to-batch variability would significantly enhance band-gap engineering in large-scale manufacturing. In the effort to discover and develop next-generation QDs, there exists a significant need for the development of automated robust strategies that rapidly explore the large parameter space (both continuous and discrete variables) associated with the synthesis of QDs and simultaneously deliver high quality, application-ready nanoparticles.[13,14]

Although conventional flask-based strategies have been the main driving force for the discovery and studies of QDs over

[a] *Department of Chemical and Biomolecular Engineering, North Carolina State University, 911 Partners Way, Raleigh, USA.*
E-mail: abolhasani@ncsu.edu; Web: https://www.abolhasanilab.com/
[b] *Department of Chemical Engineering, Massachusetts Institute of Technology, 77 Massachusetts Avenue, Building 66-525, Cambridge, MA 02139, USA*

† Electronic supplementary information (ESI) available: Liquid plug detection scheme, software process flow chart, sample of *in situ* obtained spectra, and a TEM image of synthesized perovskite QDs. See DOI: 10.1039/c7lc00884h

the past three decades,[15,16] approaching characterization, screening, and optimization of QDs with a manual batch system presents inherent limitations in sampling rate, reagent volume, and analysis time.[17,18] Furthermore, scale-up from batch synthesis for large-scale manufacturing of high-quality QDs often amplifies existing mixing inefficiencies and well-known batch-to-batch variation that can further affect the resulting products through variable and unfavorable heat and mass transfer kinetics. In the case of inorganic halide perovskite QDs (*e.g.*, cesium lead trihalide), nucleation and growth kinetics occur on the order of seconds.[3,12] Therefore, it may be challenging to obtain sufficiently small Damköhler numbers (*Da*) in batch systems for accurate (*i.e.*, not mass transfer limited) reaction kinetics characterization, which may result in an inhomogeneous nucleation process (Fig. 1A).[19]

Over the past decade, microfluidics has been promoted as an alternative strategy towards addressing the previously-mentioned challenges associated with conventional flask-based systems.[20–24] Single-phase microfluidic strategies, while superior to batch systems in chemical consumption and sampling efficiency, are oftentimes limited to laminar flow regimes with an unwanted axial dispersion, which can restrict mass transfer to radial diffusion.[25] In contrast, micro-scale multi-phase flow has been demonstrated to achieve substantially shorter mixing timescales on the order of 1 ms due to two axisymmetric recirculation patterns formed within the moving droplets.[26] The enhanced mixing and mass transfer characteristics of multi-phase microfluidics makes it an ideal option for high-throughput screening and inline optimization of the synthesis of colloidal nanocrystals (Fig. 1B). Recently, different multi-phase microfluidic strategies including combinatorial sampling,[27] three-phase flow format,[28] single droplet oscillatory flow method,[29] and chip-based approaches,[30–33] have been developed for the labor- and material-efficient characterization and screening of various colloidal semiconductor nanocrystals as well as scaled-up synthesis.[34] It should be noted, however, that consistency in plug formation and flowrates within numbered-up nano-manufacturing platforms presents a critical parameter with respect to uniform mixing and mass transfer characteristics.[35–38]

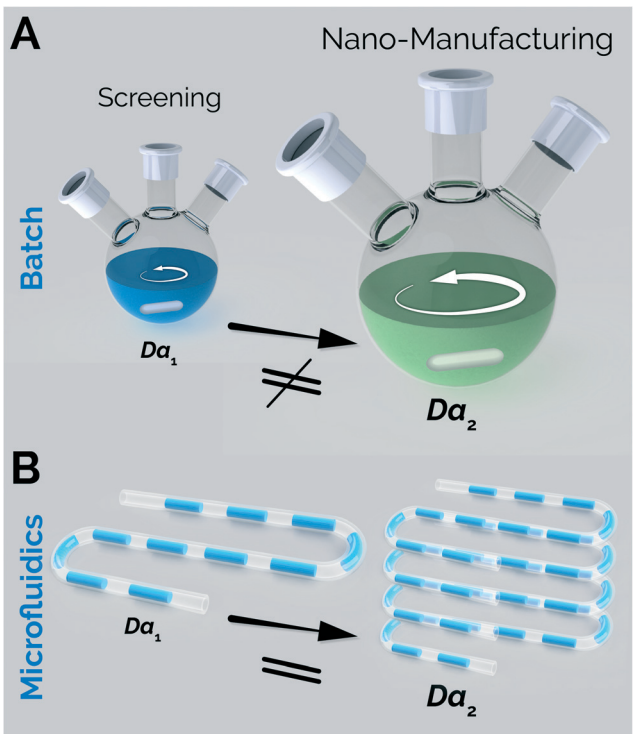

Fig. 1 Mixing and mass transfer limitations of (A) batch systems compared to (B) multi-phase microfluidic strategies for screening and large-scale manufacturing of colloidal semiconductor nanocrystals.

In situ microfluidic studies of nanomaterials synthesis are typically performed using a single detection point attached to the reactor outlet (*e.g.*, UV-vis, fluorescence, or IR spectroscopy) with a constant length reactor segment.[20] Time-dependent data are then obtained by varying flow rates within this stationary system. However, the direct correlation between the mixing timescale and the average flow velocity of multi-phase microfluidic strategies, combined with the strong dependency of the formation of nanocrystal nuclei to the degree of mixing, would result in temporal spectral measurements obtained under significantly different mixing characteristics.

In this work, we report the first modular microfluidic platform that is ideal for *in situ* screening and optimization of the synthesis of colloidal nanocrystals with both fast and slow kinetics at the synthesis temperature through controlled mixing. Utilizing a custom-designed, translating flow cell we demonstrate a significant improvement in sampling efficiency over stationary flow cell systems by obtaining up to 40 unique sample spectra associated with 20 unique residence times within a single equilibrated flow reactor at a constant mixing timescale. Next, as a case study, we characterize the relatively fast colloidal synthesis of cesium lead trihalide QDs to address the impact of mixing timescale (through adjusting the flow velocity) across both single and multi-phase systems as it pertains to nanocrystal growth and final product quality.

Experimental

Materials

Cesium hydroxide solution (50 wt% in H_2O ≥ 99.9% trace metals basis), lead(II) oxide (≥99.9% trace metals basis), tetraoctylammonium bromide (98%), and oleic acid (technical grade 90%), were purchased from Sigma-Aldrich. Toluene (99.85% extra dry over molecular sieves) was purchased from ARCOS Organics.

Precursor preparation and synthesis

The precursor preparation and perovskite synthesis were adapted from the procedures reported by Wei *et al.*,[8] with minor modifications to better suite mixing analyses and continuous flow experiments.

Precursor 1 (cesium–lead). 3 mL of a high-concentration Cs–Pb solution was prepared by first heating 0.6 mmol cesium hydroxide, 0.6 mmol lead(II) oxide, and 3 mL oleic acid in an 8 mL vial at 160 °C until a clear solution was formed (approximately 15 minutes), followed by heating at 120 °C for 1 hour. 0.0021 M Cs–Pb precursor used in syntheses was prepared by further diluting 0.5 mL of the high concentration solution with 47.5 mL of toluene in a sealed 50 mL vial.

Precursor 2 (bromide). 15 mL of the 0.013 M Br precursor solution was prepared by dissolving 109 mg tetraoctylammonium bromide in 1 mL oleic acid and 14 mL toluene in a sealed 20 mL vial then vigorously stirring until a clear solution was obtained.

Both single and multi-phase flow syntheses were performed by continuously flowing the two precursors at a 6.4 : 1 – (precursor 1) : (precursor 2) volumetric ratio. Flow equilibrium in the microreactor was assumed to occur after waiting three residence times for the furthest sampling port. Comparative batch syntheses were performed by swiftly injecting the Br solution into a quickly stirring (700 rpm) Cs–Pb precursor solution in the same volumetric ratio used in flow synthesis.

Reactor design

The modular screening platform, shown in Fig. 2, consists of an adjustable length of off-the-shelf Teflon tubing (Microsolv, fluorinated ethylene propylene (FEP), 0.125″ OD, 0.04″ ID), a custom-designed translating three-port flow cell, a collection of modular flow cell tracks with sampling ports, and a raised support structure on each end of the reactor length. The support structures, flow cell, and sampling tracks are each custom machined in aluminium (ProtoLabs), and the modular reactor extensions are 3-D printed in a stereolithography resin (methacrylate photopolymer resin, Formlabs Form 2, 0.025 mm layer resolution). The reconfigurable microreactor system may operate under both single and multi-phase flow formats. Single-phase flow experiments incorporate an off-the-shelf T-junction (IDEX Health & Science, 1/16″ PEEK), shown in Fig. 2B, while multi-phase flow experiments utilize a custom-designed PEEK four-way junction with a T-junction combination of precursors followed by a Y-junction plug formation with an inert gas (10 psig, nitrogen), shown in Fig. 2C. Operation of the automated microreactor system is carried out through a custom-developed LabVIEW script to control three syringe pumps (Harvard Apparatus, PHD Ultra), a 30 cm translational stage with a maximum linear velocity of 5 cm s^{-1} (Thorlabs, LTS300), fiber-coupled fluorescence and absorption characterization light sources (Thorlabs, M365LP1; Ocean Optics, DH-2000BAL), and a fiber-coupled photospectrometer (Ocean Optics, Flame miniature spectrometer). The LabVIEW process flow chart is provided in ESI,† S-1. The ratio of the precursors was adjusted by controlling the volumetric flow rates of precursor 1, Q_1, and precursor 2, Q_2. The size of the liquid plugs was tuned by adjusting the relative flow rates of the continuous phase (*i.e.*, pressurized nitrogen), Q_G, to the total liquid phase, Q_L

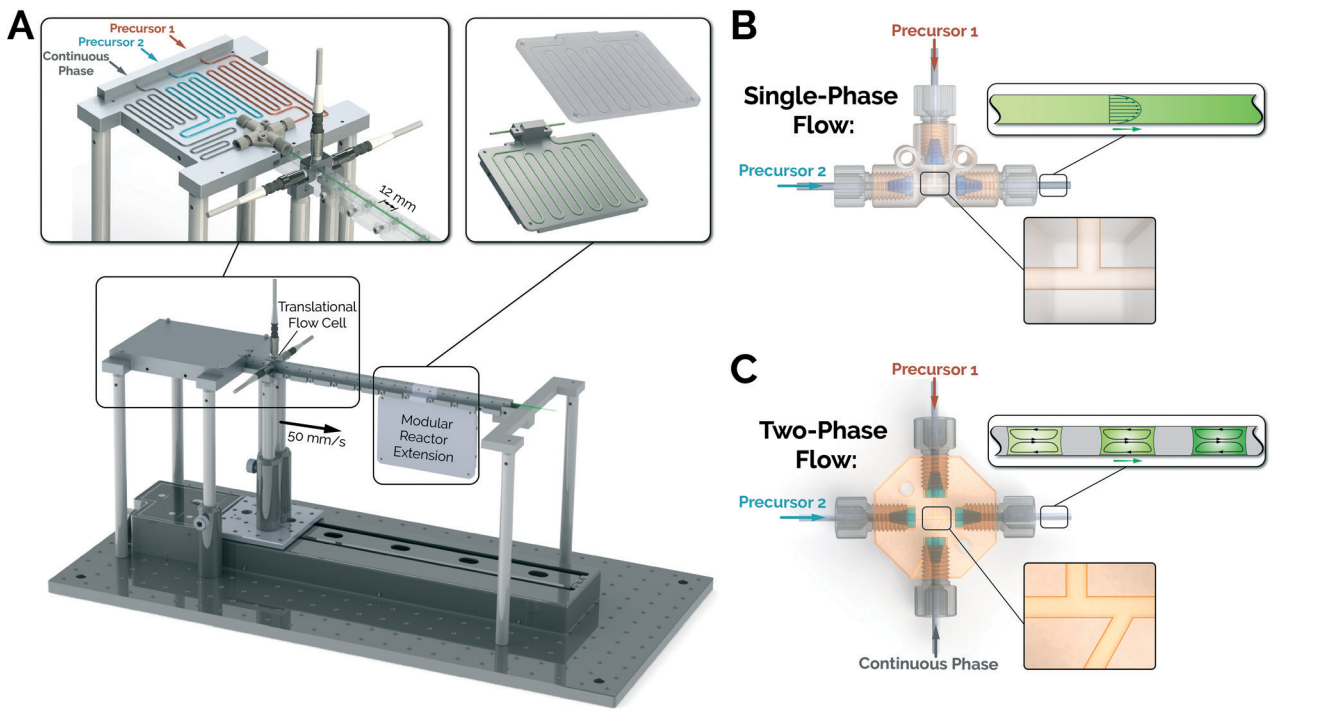

Fig. 2 (A) Schematic illustration of the automated and modular microfluidic platform with the three-port translational flow cell and the optional extension module. (B) Schematic of the standard T-junction for the single-phase flow and (C) the custom-designed four-way junction for the multi-phase flow format implementing a Y-junction plug formation.

= Q_1 + Q_2. Upon reaching equilibrium at the desired feed conditions, the translational stage automatically positions the three-port flow cell along each of the 20 sampling ports (see ESI† Video M1). Absorption and PL pathlength corrections are applied to take into account the port-to-port variations (see ESI,† Fig. S2 and S3). Upon reaching a preregistered port position, the stage is temporarily stopped and a light-source toggle sampling system, shown in Fig. 3, is applied. The sampling of a single condition includes an average across ten individual spectra for both absorption and photoluminescence, and it may complete in as little as 400 ms. Sampling times for multi-phase flow is dependent upon the specific condition flow rates – *i.e.*, the duration of time required for at least two plugs to pass the sampling port.

The designed modular microfluidic system can be adjusted to capture desired nanocrystal growth characteristics across a large range of average fluid velocities (0.6 mm s^{-1} – 13 cm s^{-1}). With the reactor extension modules, samples can be taken from 3 to 196 cm of microreactor length, while variable fluid flow rates within this modular system allow for residence times to span across four orders of magnitude, from 100 ms to 17 min. The adjustable microreactor length (achieved by extension modules in combination with the translational three-port flow cell) make the developed microfluidic platform an ideal strategy for systematic characterization of mixing properties attributed to differences in fluid velocity at equivalent residence times. By rapidly sampling up to 40 unique ports for a single equilibrated flow condition, the microfluidic platform requires on average 2 μL of precursors for each unique spectrum and may acquire up to 30 000 spectra corresponding to 15 000 experimental conditions within a single day.

Results and discussion

Plug detection

In a microscale multi-phase flow format, continuously obtained spectral data at every detection point changes significantly as different phases move across the sampling port (*cf.* Fig. 4). Not only do the corresponding PL and absorption spectra between the continuous (gas) and the dispersed (liquid) phases vary, but the refractive properties at their curved interface can substantially alter the resulting spectral data. Averaging spectra across multiple plugs is an acceptable response to this variability, and it is certainly a reasonable and necessary approach while operating at relatively high average velocities (see ESI† Fig. S4). However, in lower plug velocity conditions, averaging spectra over a long integration time becomes a significant limitation in terms of sampling time and precision, as more time is required for an equivalent volume of liquid sample to pass the sampling point. To address this sampling constraint, spectral characterization in low flow rate systems ($U_{ave} \leq 11$ mm s^{-1}) implemented a plug detection algorithm, which applies local variance calculations to continuously sampled spectra in order to find the stabilized region within a single liquid plug. The plug detection scheme then selected the ten optimal spectra within the continuous sampling timespan and averaged them together (see ESI,† Fig. S4 and S5). This technique enabled consistent and equivalent spectra collection in a fraction of the time required otherwise.

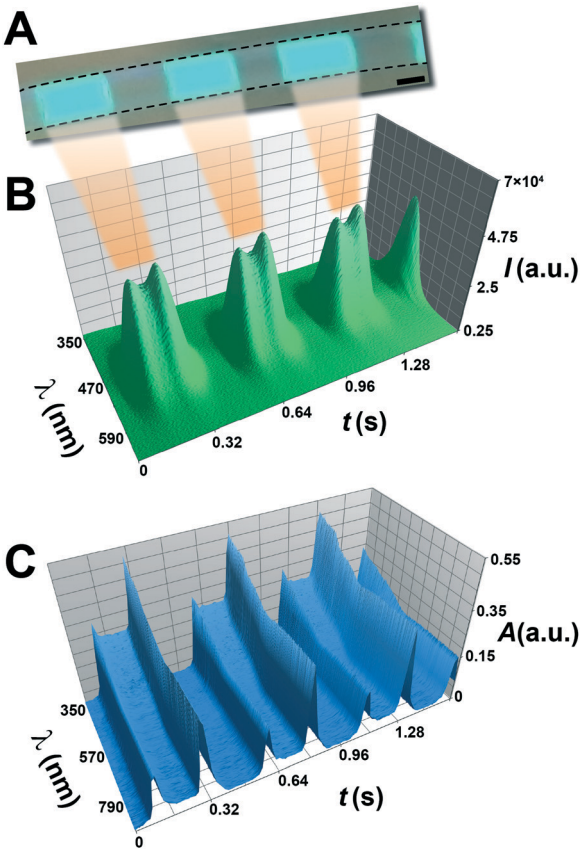

Fig. 4 (A) Fluorescence image of gas–liquid segmented flow under UV illumination and the corresponding, continuously collected (B) PL and (C) absorption spectra at one of the sampling ports along the microreactor shown in Fig. 2. Gas phase: pressurized nitrogen (10 psig) at Q_G = 278 μL min^{-1}; liquid phase: toluene containing perovskite QDs at Q_L = 185 μL min^{-1}. Integration times of 4 ms and 15 ms were used for PL and absorption spectra shown in graphs (B) and (C), respectively. Scale bar is 1 mm.

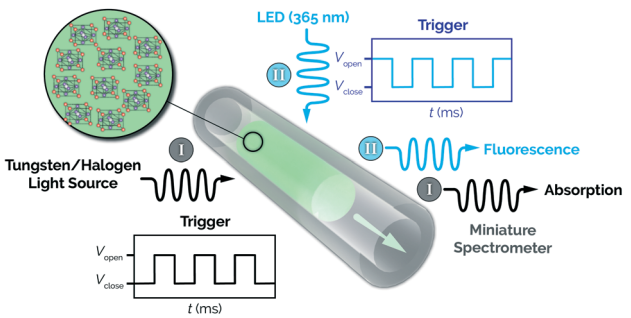

Fig. 3 Schematic of the toggle switching strategy used for the automatic acquisition of both absorption and photoluminescence spectra of in-flow synthesized perovskite QDs using the same fiber-coupled miniature photospectrometer.

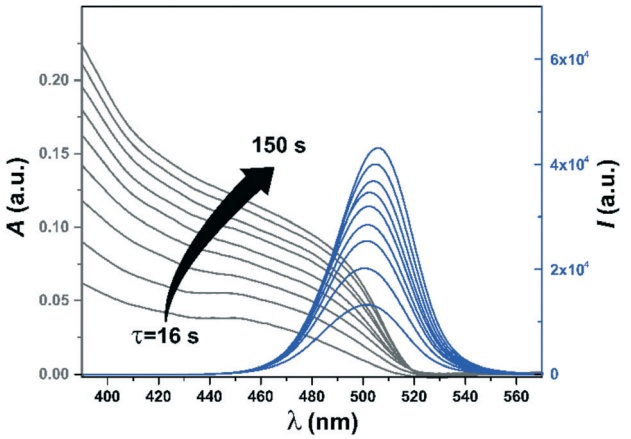

Fig. 5 Sample of *in situ* obtained absorption and PL spectra of $CsPbBr_3$ QDs for a single total flow rate condition operated in the multi-phase flow format over multiple residence times (*i.e.*, various sampling ports along the microreactor). Pressurized nitrogen (10 psig) was used as the continuous phase. Experimental conditions were Q_1 = 32 μL min^{-1}, Q_2 = 5 μL min^{-1}, Q_G = 52 μL min^{-1}. Integration times of 4 ms and 15 ms were used for PL and absorption spectra, respectively. Maximum velocity of 5 cm s^{-1} was used for the periodic movement of the translational flow cell. Data were collected within a single pass of the translational flow cell.

Nanocrystal growth and proliferation can be monitored using the PL and absorption spectra obtained at a single pass of the translating flow cell at each equilibrated flow rate. Fig. 5 shows an example of *in situ* obtained time-evolution of the absorption and PL spectra of $CsPbBr_3$ QDs synthesized at a constant average flow velocity, U_{ave} of 1.8 mm s^{-1}. The temporal spectra data obtained at different residence times (*i.e.*, different sampling ports) at a constant total average flow velocity ensures the obtained emission band-gaps and average concentration of the formed nanocrystals at different growth times are not affected by the variation in the degree of mixing. Thus, the translational three-port flow cell, for the first time, can provide spectral information regarding the synthesis of colloidal nanocrystals with similar mixing and mass transfer characteristics during the synthesis period. The increase in the absorbance of $CsPbBr_3$ QDs within the liquid plugs along the flow direction, shown in Fig. 5, corresponds to the increase in concentration (formation of new nuclei) over time. Growth of the area under PL curves further confirms the formation of more nanocrystals, while the gradual red-shift of the first excitonic peak wavelength of the absorption spectra as well as PL peak wavelength (λ_P) from 502 nm at 16 s to 507 nm at 150 s suggests a slow growth of the nanocrystals over longer reaction timescales than previously explored.[8,9,39,40]

Case study: effect of mixing on the formation of perovskite QDs

To demonstrate the versatility of the developed modular microfluidic platform, we utilized the translational three-port flow cell to study the effect of early stage mixing of

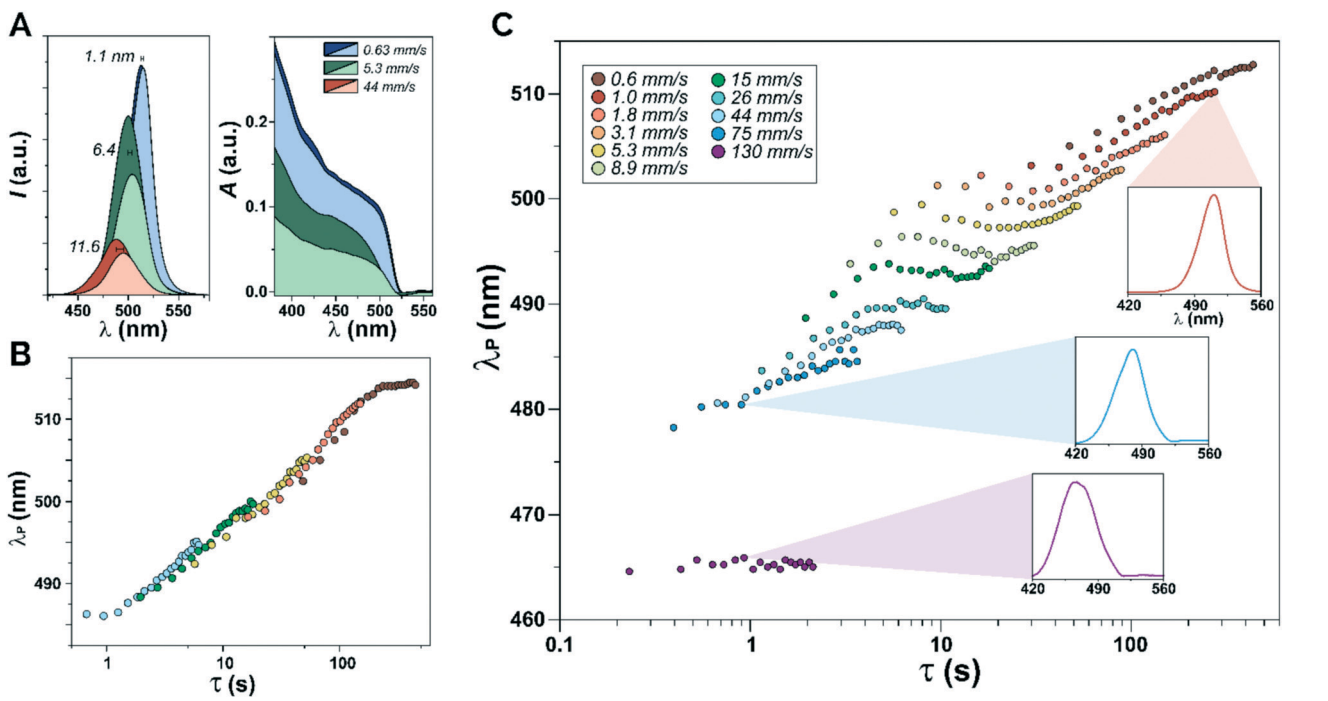

Fig. 6 (A) *In situ* obtained PL and absorption spectra of $CsPbBr_3$ QDs for single (light) and multi-phase (dark) flow formats at a 27.6 cm reactor length with the change in PL peak wavelength across three different average fluid velocities. Note that the measured absorption spectra at 44 mm s^{-1} were below the detection limit of the photo spectrometer (<0.05 a.u.). PL peak wavelength time-evolution as a function of residence time over varying average fluid velocities for (B) single and (C) multi-phase flow systems. All spectra were collected across the full modular reactor without extension units. Integration times of 4 ms and 15 ms were used for the obtained PL and absorption spectra, respectively.

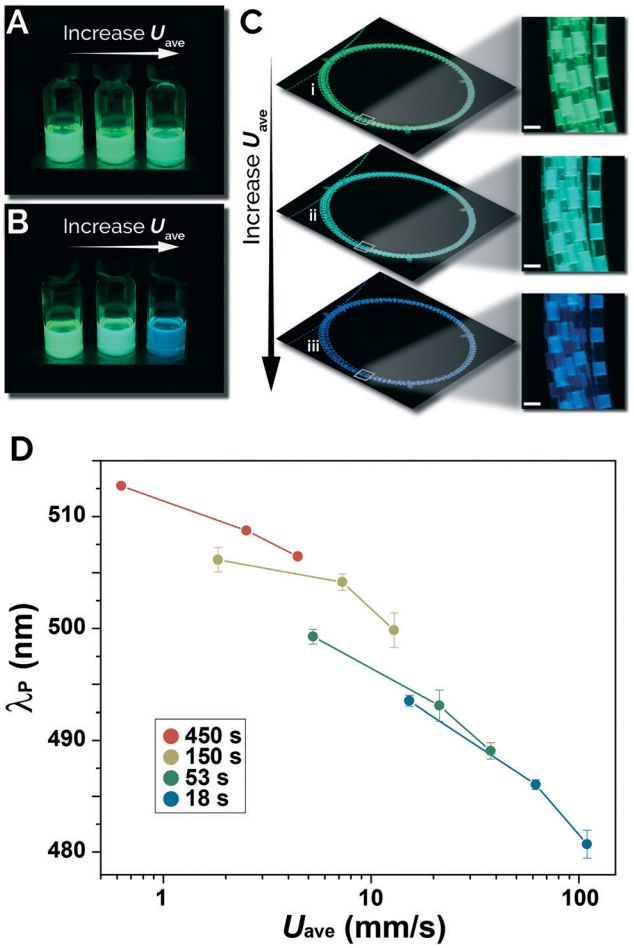

Fig. 7 Fluorescence images of collected colloidal $CsPbBr_3$ QDs under UV illumination, synthesized using the (A) single and (B) multi-phase flow formats at average flow velocities of 1.0, 3.1, and 15 cm s^{-1} through (C) 5 m of 1/16″ FEP tubing with an ID of 0.04″ (A and B images were taken approximately 30 min after synthesis, and C images were taken 15 s after halting flow). Scale bars are 2 mm. (D) Illustration of the effect of inter-phase mixing timescale on the PL peak wavelength of $CsPbBr_3$ QDs as a function of the average flow velocity over four residence times using the multi-phase flow system. Each set of constant residence time data was sampled at reactor lengths of 28, 112, and 198 cm through the incorporation of extension modules. An integration time of 4 ms was used for the detection of PL peak wavelengths.

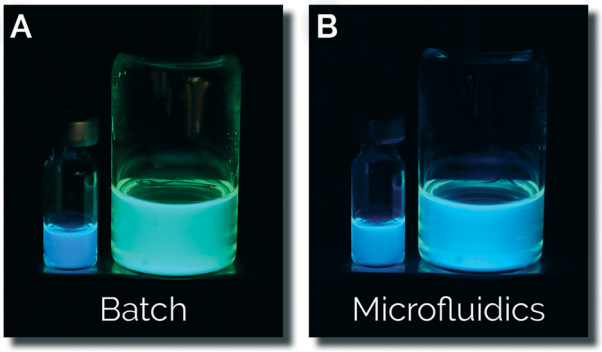

Fig. 8 (A) Demonstration of batch $CsPbBr_3$ QD synthesis variability within 2 mL and 20 mL vials compared with (B) an equivalent volume of multi-phase microfluidic products under UV illumination.

precursors on the emission band-gap of $CsPbBr_3$ QDs. We demonstrate this relationship through several methods. First, as shown in Fig. 6A, absorption and PL spectra of in-flow synthesized $CsPbBr_3$ QDs at similar residence times (*i.e.*, growth times) along the microreactor were compared between single and multi-phase flow formats. At the relatively low average flow velocity of 0.63 mm s^{-1}, corresponding to a residence time of 450 s, only a slight λ_P difference of 1.1 nm was observed between the single and multi-phase flow formats, suggesting similar mixing characteristics for both systems. But, as the average flow velocity was increased to 44 mm s^{-1}, the variation of PL peak wavelength between the single and multi-phase flow formats became an order of magnitude larger, increasing to a 11.6 nm difference at a residence time of 6.2 s. Furthermore, the corresponding absorption spectra demonstrated a higher $CsPbBr_3$ concentration (absorbance) when transitioned to multi-phase flow at a similar residence time. The results shown in Fig. 6A suggest that inter-phase mixing and mass transfer characteristics greatly influence the emission band-gap and concentration of the synthesized $CsPbBr_3$ QDs. As the average flow velocity decreases, mass transfer within both single and multi-phase flow systems becomes closer to the diffusive regime, however, by increasing the average flow velocity, the convective mixing due to the formed recirculatory patterns within the multi-phase plugs begins to significantly enhance inter-phase mixing, further separating multi-phase nanocrystal properties from that of equivalent single-phase systems. The enhanced mixing characteristics offered by multi-phase flow enables the production of a higher bulk concentration of blue-shifted particles compared to that found in single-phase products (Fig. 6A). Capitalizing on the modularity of the designed microfluidic platform, the same *in situ* screening of the colloidal synthesis of $CsPbBr_3$ QDs, shown in Fig. 6A, can be conducted at any arbitrarily selected reactor length varying between 3 to 300 cm. This phenomenon is further demonstrated with an extensive screening of the λ_P at similar average flow velocities across both single and multi-phase systems, shown in Fig. 6B and C, respectively. An example of three sets of *in situ* obtained absorption and PL spectra of $CsPbBr_3$ QDs is shown in the ESI,† S-6. As expected, no significant difference was observed between the PL peak wavelength of $CsPbBr_3$ QDs in single-phase flow systems at equivalent residence times across variable average flow velocities. Thus, a continuous relationship between residence time and emission band-gap of $CsPbBr_3$ QDs was observed in single-phase flow systems (Fig. 6B). Testing in multi-phase flow, however, demonstrated a far greater impact of the average fluid velocity on the emission band-gap of $CsPbBr_3$ QDs. Perovskite nanocrystals synthesized in multi-phase flow systems followed significantly distinct growth paths across different average flow velocities (Fig. 6C). As can be seen in Fig. 6C, higher average flow velocities (*i.e.*, faster mixing timescales) produced QDs with a

lower PL peak wavelength corresponding to a higher emission band-gap. A PL peak wavelength difference as great as 25 nm at equivalent residence times was observed for $CsPbBr_3$ QDs synthesized using different average flow velocities in the multi-phase flow system.

We further evaluated the stability, dependency, and control of the emission band-gap of $CsPbBr_3$ QDs through the collection and imaging of flow samples, shown in Fig. 7. Synthesized $CsPbBr_3$ QDs using single phase flow format at different values of U_{ave} resulted in colloidal solutions with similar emission band-gaps (*i.e.*, fluorescence colors), shown in Fig. 7A, that is consistent with the independence of the PL peak wavelength of $CsPbBr_3$ QDs to the average flow velocity of single-phase flow system shown in Fig. 6B. However, the synthesized $CsPbBr_3$ QDs using the multi-phase flow system (see ESI,† Fig. S7) resulted in distinct emission band-gaps at different average fluid velocities (*i.e.*, different inter-phase mixing characteristics). Next, by applying variable reactor lengths within the automated microfluidic platform using the extension modules, we studied the correlation between the average flow velocity of multi-phase flow systems and the PL peak wavelength of $CsPbBr_3$ QDs, shown in Fig. 7D. This result further supports the claim that early mixing kinetics greatly influence the nucleation and growth pathway of perovskite nanocrystals as well as their physicochemical properties at later time scales. Thus, the QD products of conventional batch synthesis approaches will have significant variability (Fig. 8A) due to variable mass transfer timescales and different *Da* values at early injection times across different scales (*e.g.*, small vial *vs.* big flask). In contrast, the developed multi-phase microfluidic strategy provided consistent and reproducible mixing and mass transfer characteristics and was, therefore, capable of producing QDs with similar emission band-gaps at different throughputs (Fig. 8B).

Conclusions

In conclusion, we designed and developed a fully automated modular microfluidic platform for fundamental and applied studies of the large parameter space associated with the colloidal synthesis of semiconductor nanocrystals. The developed three-port translational flow cell integrated with the modular microfluidic platform enabled access to a parameter space that was previously inaccessible using conventional microreactors. Using the modular microreactor setup, we demonstrated a rapid and effective characterization of the reaction conditions for a case study of $CsPbBr_3$ QDs. Data was collected at a rate and chemical consumption vastly superior to that of traditional batch screening methods, which enabled sampling to occur across a much wider range and higher frequency than what would be attainable otherwise. Through simultaneous collection of both absorption and PL spectra of $CsPbBr_3$ QDs along the full length of the microreactor, for the first time, we established a more accurate representation of the nanocrystal growth at a constant flow velocity (*i.e.*, similar inter-phase mixing timescale) system. In addition, *in situ* spectral monitoring of controlled nanocrystal growth, across 4 orders of magnitude reaction timescales enabled the development of the correlation between the final nanocrystal properties (emission band-gap) and the early stage reaction kinetics. Utilizing the modular microfluidic platform, we demonstrated a kinetic phenomenon both inherent to the selected perovskite synthesis and vital to improving our understanding of certain nanocrystal formations.

The developed microfluidic platform allows for additional high-throughput characterization across a wide range of reaction conditions, including but not limited to gradient changes in precursor compositions and ratios as well as the synthesis temperature. The generalized format of the developed modular platform allows for the same system to be applied to screening additional colloidal nanocrystal syntheses (*e.g.*, metal nanocrystals), enabling significantly improved material- and time-efficient characterization. Further application of the developed modular setup in conjunction with an effective numbered-up multi-phase flow platform would allow for an enhanced real-time optimization of the synthesis and optical properties of colloidal nanocrystals, thereby improving the rate of product optimization and discovery as well as the production quality in large-scale nano-manufacturing of semiconductor nanocrystals.

Conflicts of interest

There are no conflicts to declare.

Acknowledgements

The authors gratefully acknowledge the financial support provided by North Carolina State University. MA and RWE gratefully acknowledge financial support from the UNC Research Opportunities Initiative (UNC-ROI) grant.

Notes and references

1 H. Wang, H. Nakamura, M. Uehara, Y. Yamaguchi, M. Miyazaki and H. Maeda, *Adv. Funct. Mater.*, 2005, **15**, 603–608.
2 J. Pan, A. O. El-Ballouli, L. Rollny, O. Voznyy, V. M. Burlakov, A. Goriely, E. H. Sargent and O. M. Bakr, *ACS Nano*, 2013, **7**, 10158–10166.
3 S. Hou, Y. Guo, Y. Tang and Q. Quan, *ACS Appl. Mater. Interfaces*, 2017, **9**, 18417–18422.
4 A. M. Nightingale and J. C. de Mello, *ChemPhysChem*, 2009, **10**, 2612–2614.
5 G. Li, H. Wang, Z. Zhu, Y. Chang, T. Zhang, Z. Song and Y. Jiang, *Chem. Commun.*, 2016, **52**, 11296–11299.
6 S. Sun, D. Yuan, Y. Xu, A. Wang and Z. Deng, *ACS Nano*, 2016, **10**, 3648–3657.
7 G. Nedelcu, L. Protesescu, S. Yakunin, M. I. Bodnarchuk, M. J. Grotevent and M. V. Kovalenko, *Nano Lett.*, 2015, **15**, 5635–5640.
8 S. Wei, Y. Yang, X. Kang, L. Wang, L. Huang and D. Pan, *Chem. Commun.*, 2016, **52**, 7265–7268.

9 L. Protesescu, S. Yakunin, M. I. Bodnarchuk, F. Bertolotti, N. Masciocchi, A. Guagliardi and M. V. Kovalenko, *J. Am. Chem. Soc.*, 2016, **138**, 14202–14205.
10 E. Yassitepe, Z. Yang, O. Voznyy, Y. Kim, G. Walters, J. A. Castañeda, P. Kanjanaboos, M. Yuan, X. Gong, F. Fan, J. Pan, S. Hoogland, R. Comin, O. M. Bakr, L. A. Padilha, A. F. Nogueira and E. H. Sargent, *Adv. Funct. Mater.*, 2016, **26**, 8757–8763.
11 E. M. Chan, R. A. Mathies and A. P. Alivisatos, *Nano Lett.*, 2003, **3**, 199–201.
12 L. Protesescu, S. Yakunin, M. I. Bodnarchuk, F. Krieg, R. Caputo, C. H. Hendon, R. X. Yang, A. Walsh and M. V. Kovalenko, *Nano Lett.*, 2015, **15**, 3692–3696.
13 S. K. Yap, W. K. Wong, N. X. Y. Ng and S. A. Khan, *Chem. Eng. Sci.*, 2017, **169**, 117–127.
14 G. Niu, A. Ruditskiy, M. Vara and Y. Xia, *Chem. Soc. Rev.*, 2015, **44**, 5806–5820.
15 C. B. Murray, C. R. Kagan and M. G. Bawendi, *Annu. Rev. Mater. Sci.*, 2000, **30**, 545–610.
16 C. B. Murray, D. J. Norris and M. G. Bawendi, *J. Am. Chem. Soc.*, 1993, **115**, 8706–8715.
17 S. Marre and K. F. Jensen, *Chem. Soc. Rev.*, 2010, **39**, 1183–1202.
18 L. Zhang and Y. Xia, *Adv. Mater.*, 2014, **26**, 2600–2606.
19 R. L. Hartman, J. P. McMullen and K. F. Jensen, *Angew. Chem., Int. Ed.*, 2011, **50**, 7502–7519.
20 I. Lignos, L. Protesescu, S. Stavrakis, L. Piveteau, M. J. Speirs, M. A. Loi, M. V. Kovalenko and A. J. deMello, *Chem. Mater.*, 2014, **26**, 2975–2982.
21 J. Il Park, A. Saffari, S. Kumar, A. Günther and E. Kumacheva, *Annu. Rev. Mater. Res.*, 2010, **40**, 415–443.
22 T. W. Phillips, I. G. Lignos, R. M. Maceiczyk, A. J. deMello and J. C. deMello, *Lab Chip*, 2014, **14**, 3172–3180.
23 I. Lignos, S. Stavrakis, A. Kilaj and A. J. deMello, *Small*, 2015, **11**, 4009–4017.
24 I. Lignos, S. Stavrakis, G. Nedelcu, L. Protesescu, A. J. deMello and M. V. Kovalenko, *Nano Lett.*, 2016, **16**, 1869–1877.
25 J. D. Tice, H. Song, A. D. Lyon and R. F. Ismagilov, *Langmuir*, 2003, **19**, 9127–9133.
26 A. Günther, M. Jhunjhunwala, M. Thalmann, M. A. Schmidt and K. F. Jensen, *Langmuir*, 2005, **21**, 1547–1555.
27 A. Toyota, H. Nakamura, H. Ozono, K. Yamashita, M. Uehara and H. Maeda, *J. Phys. Chem. C*, 2010, **114**, 7527–7534.
28 A. M. Nightingale, T. W. Phillips, J. H. Bannock and J. C. de Mello, *Nat. Commun.*, 2014, **5**, 3777.
29 M. Abolhasani, C. W. Coley, L. Xie, O. Chen, M. G. Bawendi and K. F. Jensen, *Chem. Mater.*, 2015, **27**, 6131–6138.
30 S. Krishnadasan, J. Tovilla, R. Vilar, A. J. deMello and J. C. deMello, *J. Mater. Chem.*, 2004, **14**, 2655–2660.
31 S.-A. Leung, R. F. Winkle, R. C. R. Wootton and A. J. deMello, *Analyst*, 2005, **130**, 46–51.
32 B. K. H. Yen, A. Günther, M. A. Schmidt, K. F. Jensen and M. G. Bawendi, *Angew. Chem.*, 2005, **117**, 5583–5587.
33 S. A. Khan, A. Günther, M. A. Schmidt and K. F. Jensen, *Langmuir*, 2004, **20**, 8604–8611.
34 A. M. Nightingale, J. H. Bannock, S. H. Krishnadasan, F. T. F. O'Mahony, S. A. Haque, J. Sloan, C. Drury, R. McIntyre and J. C. deMello, *J. Mater. Chem. A*, 2013, **1**, 4067–4076.
35 M. Al-Rawashdeh, J. Zalucky, C. Müller, T. A. Nijhuis, V. Hessel and J. C. Schouten, *Ind. Eng. Chem. Res.*, 2013, **52**, 11516–11526.
36 J. Zhang, K. Wang, A. R. Teixeira, K. F. Jensen and G. Luo, *Annu. Rev. Chem. Biomol. Eng.*, 2017, **8**, 285–305.
37 S. K. Yap, W. K. Wong, N. X. Y. Ng and S. A. Khan, *Chem. Eng. Sci.*, 2016, **169**, 117–127.
38 M. J. Nieves-Remacha, A. A. Kulkarni and K. F. Jensen, *Ind. Eng. Chem. Res.*, 2012, **51**, 16251–16262.
39 W. W. Yu, L. Qu, W. Guo and X. Peng, *Chem. Mater.*, 2003, **15**, 2854–2860.
40 J. Jasieniak, L. Smith, J. van Embden, P. Mulvaney and M. Califano, *J. Phys. Chem. C*, 2009, **113**, 19468–19474.